Available online at www.sciencedirect.com
SCIENCE DIRECT®
Journal of Nuclear Materials 343 (2005) 219–226
journal of nuclear materials
www.elsevier.com/locate/jnucmat

The effect of 800 MeV proton irradiation on the mechanical properties of tungsten at room temperature and at 475 °C

S.A. Maloy [a], M.R. James [b], W. Sommer Jr. [c], G.J. Willcutt Jr. [b], M. Lopez [d], T.J. Romero [d], M.B. Toloczko [e,*]

[a] MST-8, MS-H816, Los Alamos National Laboratory, Los Alamos, NM 87545, United States
[b] D-5, MS-K575, Los Alamos National Laboratory, Los Alamos, NM 87545, United States
[c] 342 Canyon Springs Drive, Rio Vista, CA 94571, United States
[d] NMT-11, MS G742, Los Alamos National Laboratory, Los Alamos, NM 87545, United States
[e] MS P8-15, P.O. Box 999, Pacific Northwest National Laboratory, Richland, WA 99352, United States

Abstract

For the accelerator production of tritium (APT), the accelerator driven transmutation facility (ADTF), and the advanced fuel cycle initiative (AFCI), tungsten is being proposed as a target material to produce neutrons. In this study, tungsten rods were irradiated at the 800 MeV Los Alamos Neutron Science Center (LANSCE) proton accelerator for six months. After irradiation to a maximum dose in the tungsten of 23.3 dpa at $T_{irr} = 50$–270 °C, the rods were sliced into sections, hardness tests were performed at room temperature, and compression tests were performed at room temperature and at 475 °C to assess the effect of irradiation on the mechanical properties of tungsten. The results show an increase in strength and a decrease in ductility with dose. Specimens tested at 475 °C had lower yield strength and reduced work hardening capability compared to specimens tested at room temperature.
Published by Elsevier B.V.

1. Introduction

Tungsten is being considered for use as a primary or backup neutron source in many spallation neutron source applications such as the APT [1], ADTF [2], the spallation neutron source (SNS) [3], KENS (the spallation neutron source at the High Energy Accelerator Research organization, KEK) [4] and the accelerator transmutation of waste (ATW) projects [2]. For such applications the irradiation temperature is close to the ductile-to-brittle transition temperature (DBTT) for unirradiated tungsten, which ranges from 65 to 700 °C depending on the impurity content, grain size and heat treatment of the tungsten [5–7]. Therefore, tungsten is quite notch sensitive in this temperature regime, making it difficult to measure its true tensile properties. Very often, the tungsten specimens break in the elastic region before reaching yield [8,9]. Therefore to avoid brittle fracture, the mechanical properties of tungsten in this study have been measured in compression after irradiation in a proton beam.

* Corresponding author. Tel.: +1 509 376 0156; fax: +1 509 376 0418.
E-mail address: mychailo.toloczko@pnl.gov (M.B. Toloczko).

0022-3115/$ - see front matter Published by Elsevier B.V.
doi:10.1016/j.jnucmat.2004.12.018

2. Background

The effects of irradiation on tungsten have been studied previously but have mainly concentrated on the recovery of defects in irradiated tungsten [10–16]. The irradiation temperature of the tungsten in this paper is between 50 and 270 °C. These temperatures are in the stage III recovery range for tungsten. Much debate has centered on the defects responsible for recovery in stage III. Kim and Galligan [12], present strong arguments that the irradiation-produced interstitials must be the mobile defects responsible for recovery during this stage because the measured activation energy, 1.7 eV, is too low to support vacancy migration and single vacancies are always observed after stage III recovery.

A few papers have been written on the mechanical properties of tungsten after irradiation [6,7,9,17]. In these studies, the mechanical properties were either measured in bending or in tension or inferred through hardness measurements. When the properties were measured in bending or tension (at 300 °C or below), the specimens broke in the elastic regime or fractured after very low strains at 200 °C (less than 1% uniform elongation at 200 °C [6]). In one study, the Vickers micro-hardness was measured after irradiation in a proton beam [17]. These results showed an increase in hardness from 489 to 563–583 kg/mm^2 after irradiation to a dose of 3.7×10^{20} protons (~2.4 dpa). The calculated irradiation temperature was 120–300 °C.

In this paper, the mechanical properties of tungsten are presented after irradiation in an 800 MeV, 1 mA proton beam to a maximum dose of 23 dpa. The properties were measured by means of compression testing and hardness testing performed either at room temperature or at 475 °C.

3. Experimental

High purity tungsten (99.95%) was obtained from Plansee Corporation [18] in the form of ~3 mm diameter wrought rods, hot pressed, sintered and forged from powder metallurgical material. Two different rod sizes of tungsten were irradiated. One was 2.6 mm in diameter and a second was 3.2 mm in diameter. The grain size of both unirradiated materials ranged from 20 μm to 40 μm. These rods were slip clad with either 0.25 mm thick 304 L SS tubing (for the 2.6 mm diameter rods) or 0.125 mm-thick Alloy 718 tubing (for the 3.2 mm diameter rods) and backfilled with helium. The clearance between the rod and the cladding was 0.013 mm on the radius. Bundles containing 19 rods each were held in tubes and cooled with flowing water [19]. The 2.6 mm diameter rods were irradiated for six months and the 3.2 mm diameter rods for two months with an 800 MeV, 1 mA proton beam with a Gaussian distribution (two sigma = 3.2 cm). Each tungsten rod was 10 cm long allowing the accumulation of a range of doses on each rod from the center of the rod to the ends.

The fluence determination (see results in Table 1) for the irradiated samples was performed through analysis of an activation foil package that was irradiated in the center of each clad rod. The activation foil packages

Table 1
Irradiation conditions and testing conditions for tungsten specimens

Sample no.	Dose (dpa)	Tirr (°C)	Calculated H (appm)	Calculated He (appm)	Usage	Test temperature (°C)
W1-3	21.9	250	10 300	1900	Hardness	RT
W1-5	17.6	190	8300	1500	Compression	RT
W1-6	14.9	160	7000	1300	Compression	RT
W1-7	2.8	50	1300	250	Compression	RT
W1-8	3.2	50	1500	270	Compression	RT
W1-9	3.7	50	1800	320	Hardness	RT
W1-10	4.6	60	2100	400	Compression	RT
W1-12	4.0	160	1600	290	Compression	RT
W1-13	3.8	160	1600	280	Hardness	RT
W1-16	2.8	120	1100	200	Compression	RT
W1-17	0.6	60	200	40	Compression	RT
W1-18	0.7	60	300	50	Hardness	RT
W1-19	0.9	60	400	70	Compression	RT
W1-21	1.5	80	600	110	Compression	RT
W1-22	23.3	270	11 000	2020	Compression	RT
W1-23	22.5	222	10 100	1900	Compression	475
W1-24	20.3	188	9100	1700	Compression	475
W1-25	3.0	45	1300	250	Compression	475
W1-26	4.0	50	1800	330	Compression	475

were Transmission Electron Microscopy-sized disks punched from >99.98% pure thin sheet material of Al, Fe, Co, Ni, Cu and Nb. After irradiation, the stacks were withdrawn and counted by gamma spectroscopy to quantify the isotopes produced. This provided several reactions with various cross sections and thresholds, which were used to estimate the proton and neutron group fluxes. The production rates of the isotopes were calculated by taking into account the proton beam history and the measured activity. Proton and neutron flux estimates were calculated using the MCNPX code [20]. The input fluxes were then adjusted to match the measured isotope production rates using the STAYSL2 code [21]. The revised fluxes for protons and neutrons were then folded with He, H and dpa cross-sections for the materials of interest. This firmly established the exposure parameters at the activation foil locations. The error associated with the fluxes and damage levels was estimated to be around 25%. Calculated helium and hydrogen content as a function of dose are shown in Fig. 1.

Irradiation temperatures of the clad tungsten rods were determined as a function of position along the rods using LAHET Code System [22] calculated local power densities as input. The 2.6 mm diameter rods were located in an insert with only one other materials insert in the beam ahead of it. So this peak power density was 2250 W/cm^3. The 3.2 mm diameter rods were located in an insert behind several other inserts. So this peak power density was only 1020 W/cm^3. Thus, the larger, 3.2 mm diameter rods were irradiated at lower temperatures despite their larger diameters. For both inserts, there was more than a factor of 10 difference in power density between the tungsten at the beam centerline and at the ends of the rods. Cooling water temperatures were calculated locally from measured values of the initial water temperature. The cooling water temperature (T_0) at the inlet of the bundle was 27.6 °C for the 2.6 mm diameter rods and 34.8 °C for the 3.2 mm diameter rods.

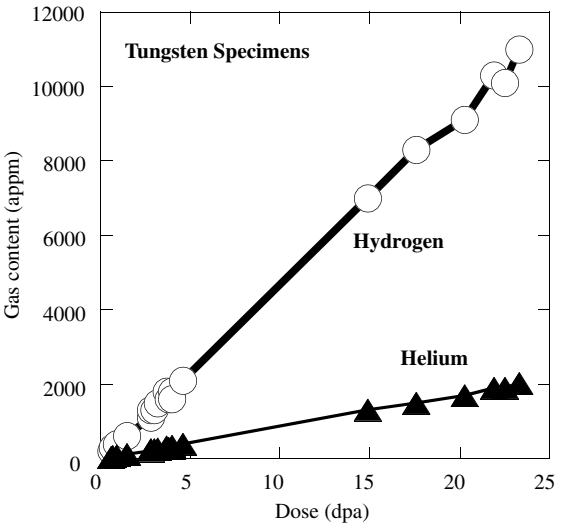

Fig. 1. Calculated helium and hydrogen content of the samples plotted as a function of dose.

Tungsten irradiation temperatures, T_{irr} (see Table 1) were calculated at each location along the rod as follows. First the heat transfer coefficient was calculated for the water flowing in the spaces between the 19 rods in the tube. The temperature drop from the clad surface to the cooling water (ΔT_{film}) was calculated by dividing the heat flux from the cladding by the heat transfer coefficient. The temperature difference across the clad thickness (ΔT_{clad}) was determined by calculating the contributions from the heat flux into the cladding from the tungsten and the power density in the cladding itself. The temperature difference across the nominal 0.013 mm helium gap (ΔT_{gap}) was calculated assuming heat transfer by conduction from the tungsten rod through the helium gas gap. The temperature rise from the tungsten rod surface to the rod centerline (ΔT_{rod}) was calculated using the tungsten power density assuming radial heat conduction through the rod. The temperature rise from the surface of the tungsten rod to the center or the rod was estimated to be no more than 5 °C. The peak tungsten temperature (T_{irr}) at each location along the rod was then calculated as

$$T_{irr} = T_0 + \Delta T_{film} + \Delta T_{clad} + \Delta T_{gap} + \Delta T_{rod}.$$

Compression specimens were prepared from one irradiated 2.6 mm diameter rod and one irradiated 3.2 mm diameter rod by slicing the rod with a slow speed diamond saw into ~3 mm long segments after it was removed from the clad capsule. The faces were then ground parallel using 600 grit SiC paper. The exact diameter and length of each specimen was measured before testing. Prior to compression testing, vacuum grease was applied to the ends of each specimen for the room temperature tests, and boron nitride was used as a lubricant for the tests performed at 475 °C. Specimens were tested in compression at an initial strain rate of 10^{-3} s^{-1} using an Instron 5567 mechanical testing machine in a hot cell. The compression tests were performed either at room temperature or at 475 °C as indicated in Table 1. Load versus crosshead displacement was measured. The compliances from the test system were mathematically removed from the displacement data. The load/displacement data were converted to engineering stress/strain data using the initial measured specimen dimensions. Some specimens, as indicated in Table 1, were mounted in epoxy and polished to finish with 1 μm diamond paste, and then, diamond pyramid hardness tests were performed on those specimens using a Leitz Metallograph with a 400 g load.

4. Test results

The engineering stress/strain curves from room temperature tests for the specimens irradiated at lower doses (up to 4.6 dpa) and over the higher dose range (4.6–23 dpa) are shown in Figs. 2 and 3, respectively. The tests in the lower dose range are divided up into specimens with a 3.2 mm initial diameter and those with a 2.6 mm initial diameter. The larger and smaller diameter specimens were made from two different heats of tungsten. Each test was stopped after accumulating ~20% plastic strain. With a few exceptions it appears that the size of the yield point is the same at each of the different irradiation doses. A slightly higher yield stress was measured for the 0 dpa, 2.6 mm diameter specimen compared to that for the 0 dpa, 3.2 mm diameter specimen. The two highest dose tests shown in Fig. 3 exhibited a decrease in load from splintering of the specimen during testing. All tests exhibited an increase in yield stress with dose.

Engineering stress/strain curves for the specimens irradiated up to 23 dpa and compression tested at 475 °C are shown in Fig. 4. All the 475 °C tests were performed on the 2.6 mm diameter specimens. Compared to room temperature tests, the magnitude of the yield stress is reduced, the magnitude of the yield drop is reduced, and the slope of the strain hardening curve is lower. The reduced slope of the strain hardening curve is due to the test temperature. As with the room temperature tests, the yield strength continually increased with dose.

Photographs were taken of the sides of the specimens after testing. No cracking was observed in the unirradiated specimens tested at room temperature. A typical

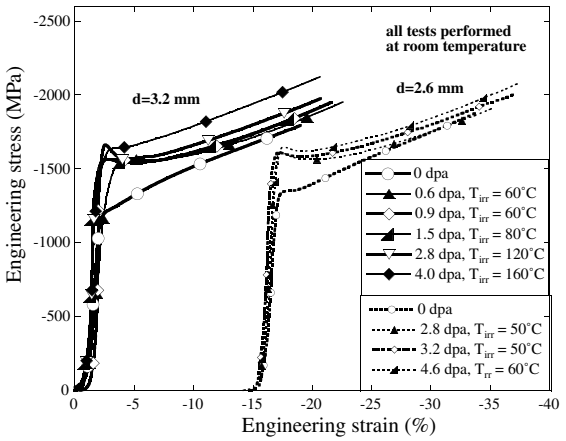

Fig. 2. Graph showing engineering stress/strain curves for tungsten irradiated to 4.6 dpa and compression tested at room temperature. Tests are divided into specimens with 3.2 mm diameter and 2.6 mm diameter. The two different size specimens were made from different heats of tungsten. Data were gathered continuously. The plot markers are an aid to distinguishing between the different tests.

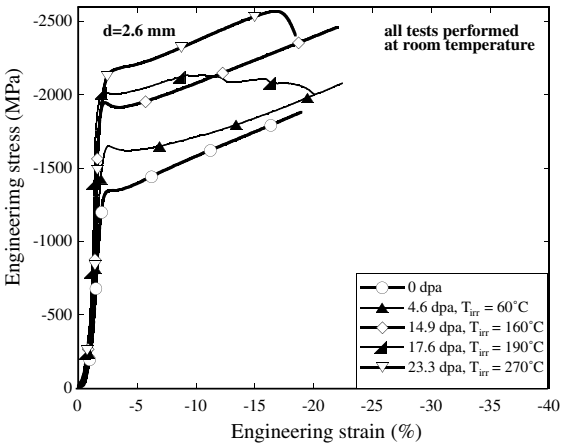

Fig. 3. Graph showing engineering stress/strain curves for tungsten tested in compression at room temperature after irradiation in a proton beam from doses ranging from 0 dpa to 23 dpa. Data were gathered continuously. The plot markers are an aid to distinguishing between the different tests.

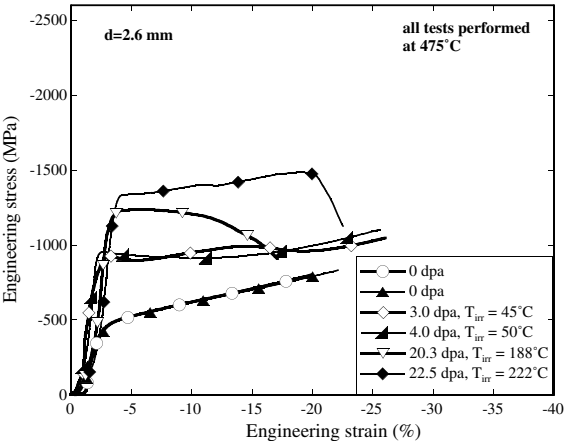

Fig. 4. Graph showing engineering stress/strain curves for tungsten tested in compression at 475 °C after irradiation in a proton beam from doses ranging from 0 dpa to 23 dpa. Data were gathered continuously. The plot markers are an aid to distinguishing between the different tests.

unirradiated specimen image after ~20% deformation at room temperature is shown in Fig. 5(a). Axial cracking was, however, commonly observed in the irradiated specimens. Examples are shown in Fig. 5(b)–(d). All irradiated specimens exhibited axial cracking after testing except for one specimen (W1-7). This was the lowest dose 2.6 mm diameter specimen (2.8 dpa) and it is possible that microcracking occurred that was not visible with the low magnification (16×) optical microscope used for analysis. Cracking was also observed in the specimens tested at 475 °C. Examples are shown in Fig. 6. At this temperature there was an increased tendency for non-uniform deformation as shown in Fig. 6(a).

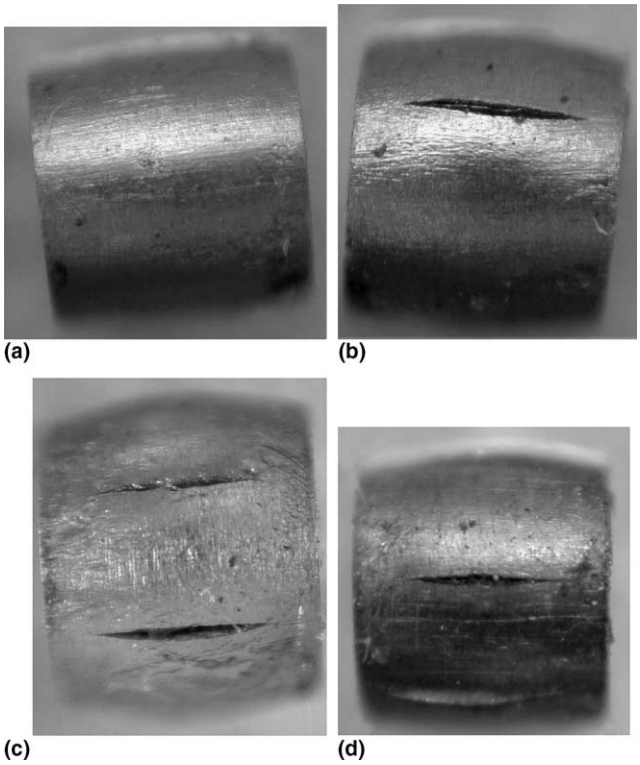

Fig. 5. Optical micrographs of tungsten compression specimens after compression to ~20% strain at room temperature, (a) before irradiation, (b) after 3.2 dpa, (c) after 14.9 dpa, and (d) after irradiation to 23.3 dpa. Pictures taken at different magnifications.

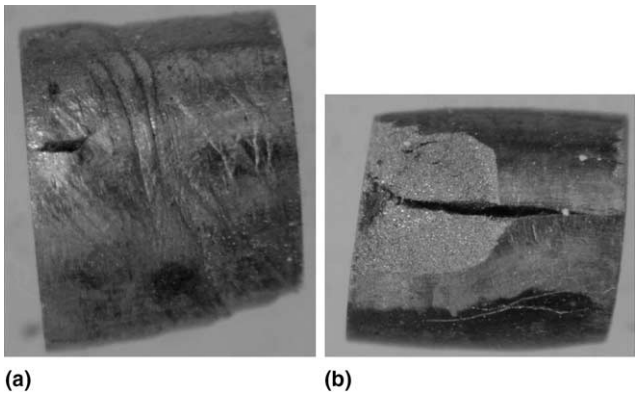

Fig. 6. Optical micrographs of tungsten compression specimens after compression deformation at 475 °C, (a) after 3.0 dpa, and (b) after 22.5 dpa. Pictures taken at different magnifications.

5. Discussion

5.1. Room temperature tests

Compression testing has been performed on annealed polycrystalline tungsten by Chen and Gray [23] at strain rates of 10^{-3} s^{-1} to 5000 s^{-1}. Our stress/strain curves on unirradiated tungsten compare well with their results for testing at a strain rate of 10^{-3} s^{-1}. Both show a yield stress between 1200 and 1400 MPa and a work hardening rate (increase in stress per unit strain) between 3150 and 3650 MPa. Although both the 2.6 and 3.2 mm diameter rods were made by the same process at Plansee Corporation, their mechanical properties were slightly

different because they came from two different heats of material. This can be seen in the 0 dpa stress/strain curves in Fig. 2. The yield stress for the 2.6 mm diameter rod is ~100 MPa higher than that measured for the 3.2 mm diameter rod. This difference is quite small and is mainly caused by the presence of a yield point in the 2.6 mm diameter rod. The work hardening rate after yielding is identical in both control materials.

The effect of increasing dose on the compression behavior can be separated into two different regimes. In the first regime, which covers doses less than 5 dpa, the yield stress value is relatively independent of dose and is about 1600 MPa. In comparing the 3.2 mm diameter specimens and the 2.6 mm diameter specimens, the difference in yield point behavior for the unirradiated materials carries over to that of the irradiated materials with the 2.6 mm diameter specimens more consistently showing a higher yield point than the 3.2 mm diameter specimens. The yield point occurs in unirradiated BCC (body-centered cubic) materials when dislocations break free from a 'solute' atmosphere formed around the dislocation core. Then, the unpinned dislocations can multiply rapidly by a multiple cross-slip mechanism [24] which results in a yield point in the stress/strain curve. A similar mechanism may be occurring in irradiated tungsten as dislocations break free from interstitials that are pinning the initial dislocations. The other regime is for doses greater than 4.6 dpa. In this regime, only 2.6 mm diameter specimens were available. An examination of the yield point behavior in both the lower dose and higher dose specimens suggests that as dose increases, the magnitude of the yield point will at some point begin to decrease. This is probably due to a radiation-induced strengthening effect reducing the yield drop following yield. In the higher dose regime, the yield strength shows a dependence on dose. The increase in yield strength can be attributed to the increase in the density of vacancies and interstitial clusters caused by irradiation. The variation in yield stress with dose over the entire range of doses is shown in Fig. 7. Although the irradiation temperature varies between 50 °C and 270 °C, this temperature change is quite small with respect to tungsten's melting temperature of 3387 °C. Thus, the range in the homologous irradiation temperature is only between 0.095 and 0.160 and this low homologous temperature range is unlikely to be responsible for the change in the mechanical response with dose observed here.

For other materials that have been irradiated at relatively low homologous temperatures in a proton irradiation environment, there is a general trend for the yield strength to initially increase rapidly with dose up to a few dpa and then increase more slowly with dose [25–28]. The proton irradiated tungsten appears to follow a similar trend for the yield strength in compression. The hardness of the tungsten as a function of dose,

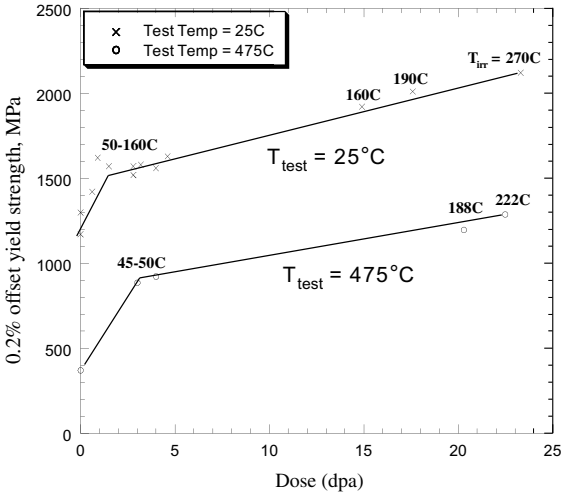

Fig. 7. Graph plotting 0.2% yield stress vs. dose for compression tests on tungsten irradiated up to 23 dpa at 50–270 °C and a test temperature of 25 °C.

as shown in Fig. 8, shows the same dependence on dose. From this, it seems probable that the same mechanisms which control the yield stress in the austenitic and ferritic/martensitic steels are also controlling the yield stress behavior in the tungsten samples. In future work, TEM analyses will be performed to investigate the relation of the irradiated tungsten microstructure to the measured mechanical properties.

The cracking observed on the sides of the compression specimens after irradiation are an indication of a decrease in ductility in tension. This decrease is probably due to: (1) the higher yield stress and higher work hardening rate, which causes a critical stress for transgranular and intergranular fracture to be reached at a lower

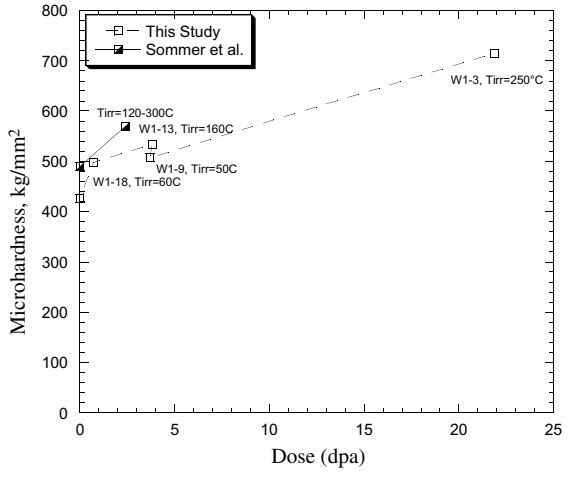

Fig. 8. Graph plotting the change in hardness with dose for tungsten after irradiation in a proton beam at 50–300 °C.

strain; and (2) irradiation-induced damage that acts a crack nucleation sites, both within grains (leading to transgranular fracture) and in grain boundaries (leading to intergranular fracture). Such a decrease in ductility has been observed in results from testing fission neutron and proton irradiated materials. Tungsten bend specimens irradiated in a 800 MeV proton beam to 2.4 dpa exhibited zero ductility (fracture in the elastic regime) at 150 °C [17]. In addition, fission neutron irradiated specimens (1×10^{21}neutrons/cm^2) exhibited zero ductility after irradiation and testing at 300 °C [9]. They also exhibited an increase in DBTT by 150 °C after irradiation at 385 °C to 9×10^{21}neutrons/cm^2 [7] and an increase in DBTT of 165 °C after irradiation to 9.5×10^{20}neutrons/cm^2 at 250 °C [29].

5.2. Discussion of 475 °C tests

For the 2.6 mm diameter samples, the size yield point in the 475 °C tests was smaller than observed in the room temperature tests. This is likely because at the elevated temperature, the increased solute diffusivity did not allow the dislocations to escape from their solute atmospheres. In the 475 °C tests, the general dependence of the yield strength of tungsten on dose is the same as that for the room temperature tests, but the magnitude of the values are lower as shown in Fig. 7. A similar result was obtained for a ferritic/martensitic steel that was tensile tested at room temperature and at 500 °C [25]. Because it is unlikely that any thermal aging occurred at 475 °C in the tungsten, the reduction in the yield strength at 475 °C is most likely due to changes in dislocation dynamics at this temperature. The reduction in the yield strength of the unirradiated material at 475 °C further supports this notion. The work hardening slope at 475 °C is also much lower, and in many instances mechanical instability occurred shortly after yield. In some instances, the mechanical instability appeared as regions of large amounts of localized compressive deformation as shown in Fig. 6(a). This localized heavy deformation will occur when a region of the sample can no longer significantly harden, either by geometric means (i.e. by further increase in cross-sectional area) or by microstructural means, more than the material above and below it. Thus, the work hardening rate of tungsten must be so low in these test conditions that not even the geometric hardening that is inherent to compression tests could prevent the localized heavy deformation. These results suggest that the tungsten may be undergoing a form of channel deformation like that which occurs in austenitic and ferritic/martensitic steels [30,31].

5.3. Helium effects

Helium content in the 20+ dpa samples was in the range of 2000 appm. Samples without helium were not available for comparison. The effect of helium on tensile properties is a current topic of discussion. There is little information on the effect of He on tungsten tensile properties, however there is some information on the effect of helium on the tensile properties of BCC steels. In one study of Eurofer97, the material was irradiated in a high energy proton environment at 250 °C to doses ranging from 0.16 to 0.47 dpa resulting in helium content ranging from about 16 appm to 47 appm [32]. The room temperature yield strength of the material after 0.47 dpa was about 675 MPa. In another study of Eurofer97, the material was helium irradiated at 250 °C to doses of almost 0.4 dpa and helium contents of 2500 appm [33]. Here, the room temperature yield strength of the material was 1100 MPa. In this rough comparison, it appears that there is evidence that large amounts of helium can affect the tensile properties of BCC steels. Its seems reasonable to conclude that helium may also be having some effect on the compressive deformation behavior of the tungsten. A proper irradiation study would be needed to obtain concrete information.

6. Conclusions

The effect of proton irradiation on the mechanical properties of tungsten has been measured by hardness and compression testing after irradiation in a proton beam to a maximum dose of 23 dpa. The results showed the following:

1. The compressive yield stress of tungsten tested at room temperature increased by a factor of 1.6 after irradiation to 23 dpa, and by more than a factor of 3 when tested at 475 °C after 23 dpa.
2. The increase in yield strength with dose has not shown any sign of saturation by 23 dpa in either the room temperature tests or the 475 °C tests.
3. Cracking was observed on the sides of compression specimens after testing suggesting a decrease in tensile ductility after irradiation.
4. The deformation behavior of some of the specimens tested at 475 °C suggests that channel deformation may be occurring in tungsten when tested at 475 °C after irradiation.

Acknowledgements

This program benefited from a large collaboration involving scientists and engineers from numerous groups at Los Alamos National Laboratory as well as a materials working group consisting of representatives from

Pacific Northwest National Laboratory, Oak Ridge National Laboratory, Sandia National Laboratories, Lawrence Livermore National Laboratory, Savannah River Technology Center, and Brookhaven National Laboratory. We are indebted to all participants. I would also like to thank Robert Margevicius for helpful review of this paper.

References

[1] M.W. Cappiello, E. Pitcher, Mater. Charact. 43 (1999) 73.
[2] S. Wender, Preliminary assessment of spallation options for accelerator-driven transmutation, AAA-RPO-TRNS-01-0017, LAUR-01-1634, Los Alamos, NM, Los Alamos National Laboratory, 2001, p. 20.
[3] S.J. Pawel, Preliminary materials recommendation for a solid target back-up for the SNS, SNS/TSR-0149, Oak Ridge, TN, Oak Ridge National Laboratory, 1999, p. 35.
[4] M. Kawai, K. Kikuchi, H. Kurishita, J. Li, M. Furusaka, J. Nucl. Mater. 296 (2001) 312.
[5] R. Koo, Trans. of the Met. Soc. of AIME 227 (1963) 280.
[6] M.J. Makin, E. Gillies, J. Inst. Metals 86 (1957) 108.
[7] J.M. Steichen, J. Nucl. Mater. 60 (1976) 13.
[8] B.L. Mordike, J. Inst. Metals 88 (1959) 272.
[9] I.V. Gorynin, V.A. Ignatov, V.V. Rybin, S.A. Fabritsiev, V.A. Kazakov, V.P. Chakin, V.A. Tsykanov, V.R. Barabash, Y.G. Prokofyev, J. Nucl. Mater. 191–194 (1992) 421.
[10] M.W. Thompson, Philos. Mag. 5 (8) (1960) 278.
[11] G.H. Kinchin, M.W. Thompson, J. Nucl. Energy 6 (1958) 275.
[12] Y.W. Kim, J.M. Galligan, Acta Metall. 26 (1978) 379.
[13] L.K. Keys, J. Moteff, J. Nucl. Mater. 34 (1970) 260.
[14] Y. Kim, J. Galligan, J. Nucl. Mater. 69&70 (1978) 680.
[15] M.S. Anand, B.M. Pande, R.P. Agarwala, Indian J. Phys. 53A (1979) 35.
[16] J. Cornelis, L. Stals, P. De Meester, J. Roggen, J. Nihoul, J. Nucl. Mater. 69&70 (1978) 704.
[17] W.F. Sommer, Tungsten materials analysis letter report, LA-UR-95-220, Los Alamos, NM, Los Alamos National Laboratory, 1995, p. 51.
[18] Plansee Corporation, A-6600 Reutte/Tirol, Austria.
[19] S.A. Maloy, W.F. Sommer, R.D. Brown, J.E. Roberts, J. Eddleman, E. Zimmermann, G. Willcutt, in: M.S. Wechsler et al. (Eds.), Materials for Spallation Neutron Sources, The Minerals, Metals & Materials Society, 1998, p. 131.
[20] H.G. Hughes, K.J. Adams, M.B. Chadwick, J.C. Comly, H.W. Egdorf, S.C. Frankle, J.S. Hendricks, R.C. Little, R. MacFarlane, R.E. Prael, L.S. Waters, M.C. White, P.G. Young Jr., F.X. Gallmeier, E.C. Snow, in: ANS Proceedings of the 2nd International Topical Meeting on Nuclear Applications of Accelerator Technology, American Nuclear Society, La Grange Park, IL, 1998, p. 281.
[21] M.R. James, S.A. Maloy, W.F. Sommer, P.D. Ferguson, M.M. Fowler, G.E. Mueller, R.K. Corzine, in: J.G. Williams (Ed.), Reactor Dosimetry: Radiation Metrology and Assessment, ASTM, West Conshohoken, PA, 2001, p. 167.
[22] R.E. Prael, H. Lichtenstein, User Guide to LCS: The LAHET Code System, LA-UR 89-3014, Los Alamos, NM, Radiation Transport Group, Los Alamos National Laboratory, 1989, p. 76.
[23] S.R Chen, G.T. Gray, in: A. Bose, R.J. Dowling (Eds.), Tungsten and Refractory Metals – 1994, Metal Powder Industries Federation, Princeton, NJ, 1994, p. 489.
[24] R.W. Hertzberg, Deformation and Fracture Mechanics of Engineering Materials, John Wiley, New York, NY, 1989, p. 122.
[25] M.B Toloczko, M.L. Hamilton, S.A. Maloy, J. Nucl. Mater. 318 (2003) 200.
[26] S.A. Maloy, M.R. James, G. Willcutt, W.F. Sommer, M. Sokolov, L.L. Snead, M.L. Hamilton, F. Garner, J. Nucl. Mater. 296 (2001) 119.
[27] Y. Dai, S.A. Maloy, G.S. Bauer, W.F. Sommer, J. Nucl. Mater. 283–287 (2000) 513.
[28] K. Farrell, T.S. Byun, J. Nucl. Mater. 296 (2001) 129.
[29] W. Lohmann, Materials investigations for the SNQ target station-progress report, 1985, Jul-2061, ISSN-0366-0855, Kernforschungslange Juelich, 1986, p. 138.
[30] Y. Dai, X. Jia, J.C. Chen, W.F. Sommer, M. Victoria, G.S. Bauer, J. Nucl. Mater. 296 (2001) 174.
[31] E.H. Lee, T.S. Byun, J.D. Hunn, K. Farrell, L.K. Mansur, J. Nucl. Mater. 296 (2001) 183.
[32] P. Spätig, R. Schäublin, S. Gyer, M. Victoria, J. Nucl. Mater. 258–263 (1998) 1345.
[33] P. Jung, J. Henry, J. Chen, J.-C. Brachet, these Proceedings, doi:10.1016/j.jnucmat.2004.11.018.